Ref. Ares(2022)3117858 - 20/04/2022

Deliverable 2.1

ENABLEH2

PUBLIC REPORT

Heat management system conceptual design tools report

ENABLE·H2

ENABLing cryogEnic Hydrogen-based CO2-free air transport

Call identifier

H2020-MG-2016-2017/H2020-MG-2017-Two-Stages

Project start

01.09.2018

Project duration

51 months

This project has received funding from the European Union's Horizon 2020 research and innovation programme under **grant agreement no 769241**

Table of Contents

1 Introduction 6
1.1 Thermophysical Properties of Jet A and LH_2 6
1.2 Heat management system 10
1.2.1 Expander cycle 11
1.3 Fuel distribution system 12
1.3.1 Boost Pump 13
1.3.2 High-Pressure Pump 14
2 Design Tools 16
2.1.1 Combustion modeling 16
2.1.2 Detailed modeling of real gases 16
2.1.3 Modeling of coupled heat management systems 17
2.1.4 Engine template for cryogenic fuels 18
2.1.5 Quantifying installation effects 18
2.2 Conceptual design of heat exchangers 19
2.2.1 Generalized approach to model compact HEX technology 19
3 Parametric study 25
3.1 Reference optimized cycle 25
3.2 Results 26
3.2.1 Pre-cooler HEX performance 29
3.2.2 Intercooler HEX performance 30
3.3 Conclusion 31
4 Bibliography 33

Notation

A	Heat Transfer Area
A_{ff}	Minimum Cross-sectional Area Perpendicular to Flow Direction
A_{ft}	Frontal Area
AC	Alternating Current
BPR	Bypass Ratio
C	Chord length
C_{max}	Maximum Heat Capacity Rate
C_{min}	Minimum Heat Capacity Rate
c_p	Specific Heat Capacity at Constant Pressure
c_v	Specific Heat Capacity at Constant Volume
CC	Cooled-cooling
CEA	Chemical Equilibrium with Applications
CHEX	Compact Heat Exchanger
CO_2	Carbon Dioxide
D	Drag, Diameter
D_h	Hydraulic Diameter
D_i	Inner Diameter of Tube
D_o	Outer Diameter of Tube
DC	Direct Current
DOC	Direct Operating Cost
F_N	Net Thrust
FAA	Federal Aviation Administration
FAR	Federal Aviation Regulations
FPR	Fan Pressure Ratio
f_d	Darcy Friction Factor
G	Maximum Mass Velocity
g	Gravity Acceleration
H_u	Net Calorific Value
HEX	Heat Exchanger
HMS	Heat Management System
HPC	High Pressure Compressor

HPT	High Pressure Turbine
h	Heat Transfer Coefficient, Enthalpy
IC	Intercooling
IGV	Inlet Guide Vane
IPC	Intermediate Pressure Compressor
ISA	International Standard Atmosphere
IUPAC	International Union of Pure and Applied Chemistry
J	Colburn j Factor
k	Thermal Conductivity
L	Pipeline Length
LH_2	Liquid Hydrogen
LNG	Liquefied Natural Gas
LPC	Low Pressure Compressor
LPT	Low Pressure Turbine
L/D	Lift over Drag Ratio
M	Mach Number, Mass
$\dot{m}$	Fuel Flow Rate
N_{tubes}	Number of Tubes
NO_X	Nitrogen Oxides
NPSH	Net Positive Suction Head
NPSP	Net Positive Suction Pressure
NTU	Number of Transfer Units
OBIGS	Onboard Inert Gas System
OGV	Outlet Guide Vane
OPR	Overall Pressure Ratio
P	Pressure
PC	Pre-cooling
Pr	Prandtl Number
q	Heat Transfer Rate
q_L	Feed Line Heat Flux per unit Length
R	Particular Gas Constant
REC	Recuperation
Re	Reynolds Number

R_{H_2}	Gas Constant
R_h	Local Hub Radius
R_t	Local Tip Radius
R_w	Tube Wall Conduction Resistance
S	Entropy
SFC	Specific Fuel Consumption
SLS	Sea Level Static
SMR	Short-Medium Range
STP	Standard Temperature and Pressure
St	Stanton Number
T	Temperature
TIT	Turbine Inlet Temperature
TSFC	Thrust-Specific Fuel Consumption
$\overline{\mathrm{TSFC}}$	Installed TSFC
U	Overall Heat Transfer Coefficient
v	Velocity
Δh	Enthalpy Change
$\Delta \mathrm{T}$	Temperature Difference
ϵ	Effectiveness
γ	Specific Heat Ratio (c_p/c_v)
η	Efficiency
λ	Heat Conductivity
μ	Dynamic Viscosity
Π_{HPC}	Compressor Pressure Ratio
Π_{pump}	Pump Pressure Ratio
ρ	Density
σ	Free-flow Area to Frontal Area Ratio

1 Introduction

The development of commercial air transportation over the coming decades [1, 2] requires greater consideration of its ecological impact concerning the emanations of greenhouse gases such as CO_2. Consequently, the traditional fossil-based jet fuel may be replaced by an economic and eco-friendly fuel emitting less CO_2, such as Liquid Hydrogen (LH_2) or Liquefied Natural Gas (LNG). These types of fuels are classified as cryogenic fuels due to their extremely low storage temperatures. Rocket engines and some experimental aircraft engines have used LH_2, but hitherto this fuel has not been considered economically viable for civil aviation. However, recent studies for utilizing cryogenic fuels, especially LH_2, in commercial aircraft have confirmed their potential to achieve 'green aviation' [3, 4, 5].

Although replacing fossil-based fuel by LH_2 might seem promising, it will challenge many established practices related to fuel systems, materials, airframe design, and propulsion technologies. For instance, a comparison of the thermophysical properties of Jet A and hydrogen shows the latter has a lower volumetric energy density (MJ/m^3) than Jet A (about 4.2 times). Hence, for a fixed amount of energy, a larger storage volume is required for LH_2 resulting in a larger body for the aircraft. In addition, the complexity of hydrogen storage in terms of insulation and supporting structures must be taken into consideration. On the other hand, the low temperature and high specific thermal capacity of LH_2 enables its cooling capacity to be exploited to improve engine efficiency.

From an environmental point of view, a comparison of exhaust emissions of kerosene and liquid hydrogen [6, 7] encourages the utilization of LH_2 as an ideal alternative fuel for aviation. It eliminates carbon dioxide, carbon monoxide, sulfur oxides, unburned hydrocarbons and soot emissions (other than those generated through oil consumption). An improved combustion stability range for lean mixtures should also contribute for a reduction in NO_x emissions. However, the hydrogen-fueled subsonic aero-engines will emit about three-times more water vapor than the Jet A fueled engines [8] and the direct and indirect impact of water vapor on the climate must also be taken into account [8, 9].

Since liquid hydrogen is stored at cryogenic temperatures it can undergo a large temperature variation on its way to the combustion chamber. That associated with the fact that hydrogen has an exceptionally high heat capacity, results that the amount of heat that can be taken up is substantial. As an example, assume that the tank operates at 25 K and the fuel absorbs heat up to 800 K entering the combustor, the heat added corresponds to 9% of the lower fuel heating value and hence gives a potential 9% Specific Fuel Consumption (SFC) reduction benefit. Different concepts for heat rejection in the compression system, such as pre-cooling and intercooling have been investigated in the past. Brewer [2] focused on comparing a wider range of options for heat management, including also recuperation and cooling of the cooling air. Brewer observed the smallest benefits for cooling the turbine cooling air, intercooling was better and precooling better still. However, the greatest benefits were observed from recuperation, indicative of that the hydrogen temperature could be pushed further by this heat source. In intercooling and pre-cooling, the temperature increase of the hydrogen is limited by the lower temperature of the compressor air.

In the present report the different tools and methods implemented to simulate the fuel architecture and heat management system are presented and discussed. Additionally, the potential for net benefits by pre-cooling and intercooling is also investigated in a parametric study.

1.1 Thermophysical Properties of Jet A and LH_2

Table 1 presents a comparison between the physical properties of kerosene and liquid hydrogen. Compared to Jet A, LH_2 has a higher heating value (approximately 2.8 times) which in turn theoretically reduces the fuel weight to a third. On the other hand, LH_2 has a much lower density than Jet A (approximately one tenth). This means that for a fixed amount of energy, more storage volume is required for LH_2. Moreover, due to the extremely low storage temperature (approx. 20 K @ 145 kPa), LH_2 tanks require careful insulation, increasing their complexity and complicating their supporting structures.

Table 1: *Physical Properties of Kerosene (Jet A) and Liquid Hydrogen (LH_2)*

Fuel	Heat of combustion [MJ kg^{-1}]	Density [kg m^{-3}]	Energy density [MJ m^{-3}]
Kerosene (Jet A)	~43.02	~820	~35396
Liquid Hydrogen (LH_2)	~120.1	~70.8	~8500

Table 2 shows the properties of hydrogen at different phases [10]. In addition, comparison for the emission species between Jet A and LH_2 is displayed in Table 3 [6]. As seen, the main benefit of using liquid hydrogen, which makes it an ideal alternative fuel, is to cut away carbon dioxide (CO_2), sulfur oxides (SO_x), Unburnt Hydrocarbon (UHC), and soot, compared with Jet A.

Table 2: *Properties of Hydrogen*

Item	Property	Value and Unit
	molar mass	2.016 kg $kmol^{-1}$
	particular gas constant	4124 J kg^{-1} K^{-1}
	(gravimetric) calorific value Hu	120 MJ kg^{-1}
@ triple point	temperature	-259.35 ºC (13.80 K)
	pressure	0.07 bar
	density gaseous	0.125 kg m^{-3}
	density liquid	77 kg m^{-3}
	heat of fusion	58.5 kJ kg^{-1}
@ boiling point at 1 atm.	boiling temperature	-252.85 ºC (20.30 K)
	heat of vaporization	445.4 kJ kg^{-1}
liquid phase as above	density	70.8 kg m^{-3}
	(volumetric) calorific value	8.5 MJ dm^{-3}
	specific heat capacity c_p	9.8 kJ kg^{-1} K^{-1}
	specific heat capacity c_v	5.8 kJ kg^{-1} K^{-1}
	thermal conductivity	0.099 W m^{-1} K^{-1}
	dynamic viscosity	11.9E-6 N s m^{-2}
	speed of sound	1089 m s^{-1}
gaseous phase as above	density	1.34 kg m^{-3}
	(volumetric) calorific value	0.16 MJ dm^{-3}
	specific heat capacity c_p	12.2 kJ kg^{-1} K^{-1}
	specific heat capacity c_v	6.6 kJ kg^{-1} K^{-1}
	thermal conductivity	0.017 W m^{-1} K^{-1}
	dynamic viscosity	1.11E-6 N s m^{-2}
	speed of sound	355 m s^{-1}
@ critical point	temperature	-239.95 ºC (33.20 K)
	pressure	13.1 bar
	density	31.4 kg m^{-3}
@ formerly IUPAC (STP) until 1982 (0 °C and 1.01325 bar)	density	0.09 kg m^{-3}
	(volumetric) calorific value	0.01 MJ dm^{-3}
	specific heat capacity c_p	14.32 kJ kg^{-1} K^{-1}
	specific heat capacity c_v	10.17 kJ kg^{-1} K^{-1}
	thermal conductivity	0.184 W m^{-1} K^{-1}
	coefficient of diffusion	0.61 cm^2 s^{-1}
	dynamic viscosity	8.91E-6 N s m^{-2}
	speed of sound	1246 m s^{-1}
mixtures with air (@ ambient temperature and pressures, approximately 25 °C and 1 atm.)	lower explosion limit	4 Vol% H_2 (λ=10.1)
	lower detonation limit	18 Vol% H_2 (λ=1.9)
	stoichiometric mixture	29.6 Vol% H_2 (λ=1)
	upper detonation limit	58.9 Vol% H_2 (λ=0.29)
	upper explosion limit	75.6 Vol% H_2 (λ=0.13)
	ignition temperature	585 °C (858 K)
	minimal ignition energy	0.017 mJ
	max. laminar flame speed	about 3 m s^{-1}
	adiabatic combustion temperature	about 2100 ºC

Table 3: *Emission species of Kerosene (Jet A) and Liquid Hydrogen (LH_2)*

Fuel	Amount consumed [kg]	CO_2 emission [kg]	H_2O emission [kg]	Other species
Kerosene (Jet A)	1.0	3.16	1.2	CO, NOx, SO_2, UHC, Soot
Liquid Hydrogen (LH_2)	0.36	0.0	3.21	NOx

These major differences between Jet A and LH_2 create lots of challenges for aircraft configuration, fuel supply systems, propulsion systems, safety and overall performance. Moreover, to improve the performance of the propulsion system while using cryogenic fuel, various concepts for advanced engine cycles must be considered.

Figure 1 presents the behavior of specific heat vs. temperature at different pressures in the vicinity of the critical point (33.2 K and 13.1 bar). For each pressure, there is a peak in the specific heat of hydrogen near the critical temperature, all isobars are diverged because of phase change from liquid to vapor [11]. At higher pressures, this sudden jump is not so pronounced. Moreover, a sharp jump only occurs close to the critical temperature and pressure. In practice, after the first heat exchanger (HEX) in the engine's cycle, the hydrogen will be above the critical temperature.

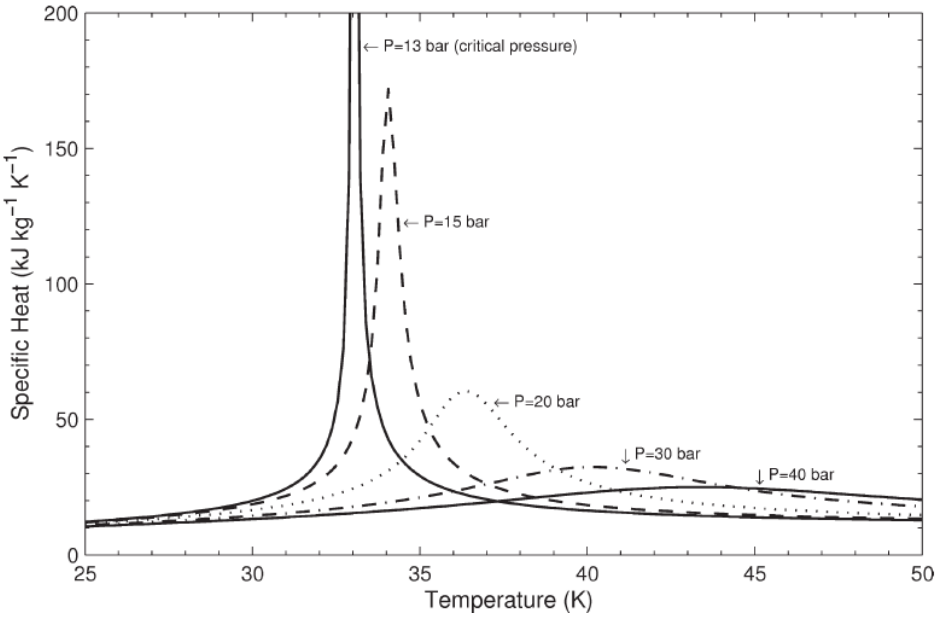

Figure 1: Specific heat of equilibrium hydrogen vs. temperature at various pressures [11].

For the thermodynamic of the fuel's performance, ranging from cryogenic conditions to high temperatures before entering the combustor, the temperature vs. entropy (T-S) diagram (see Figure 2) provides a powerful tool where the state change and work/heat transfer to/from the system cycle can be visualized.

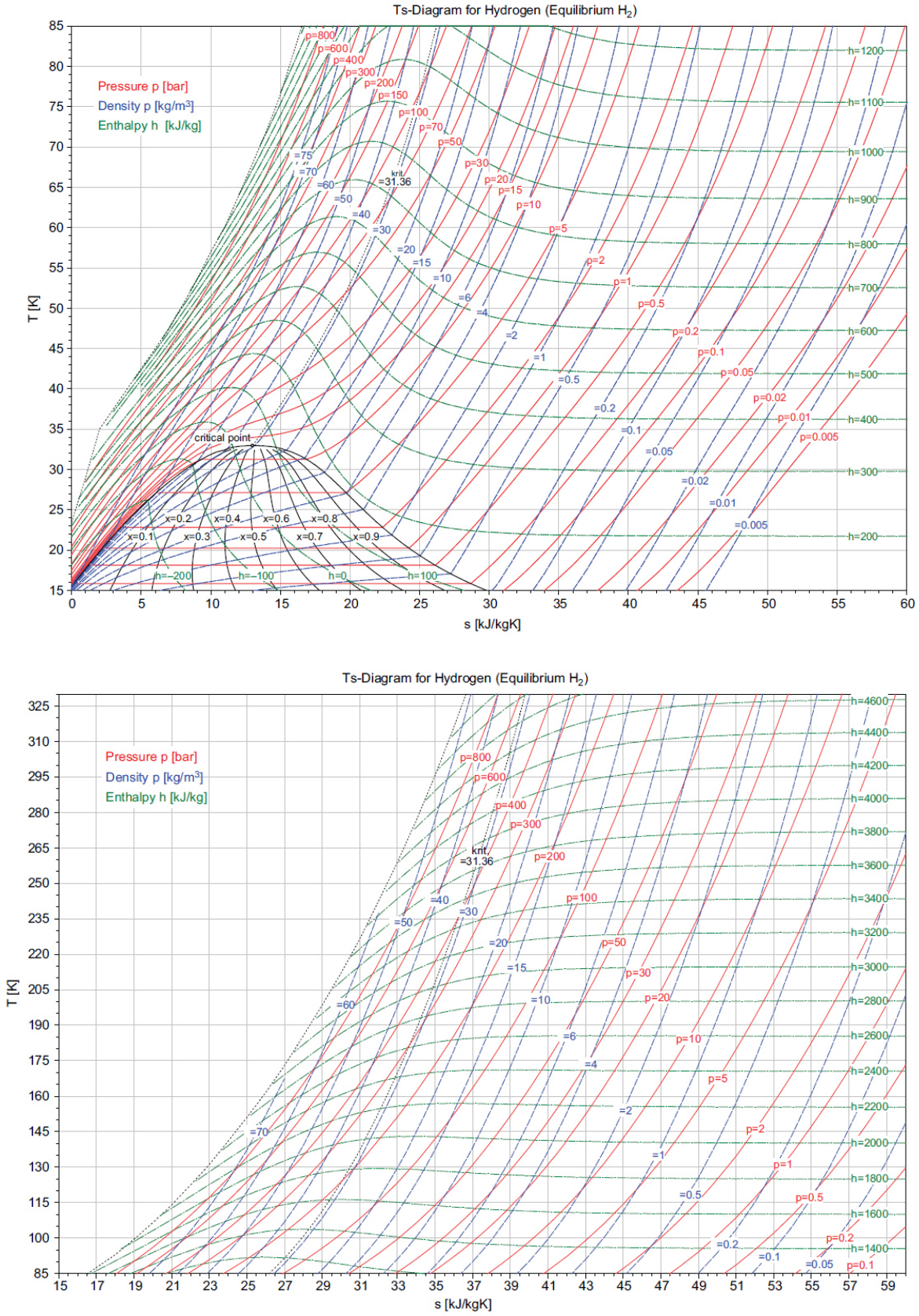

Figure 2: T-S diagram for equilibrium hydrogen for temperatures from 15 to 330 K [10].

1.2 Heat management system

The heat management system is integral to the fuel supply system and the propulsion system, where it delivers the hydrogen with appropriate pressure and temperature to the combustion chamber. The very low temperature of the LH_2 means that it could potentially undergo a large temperature change on its way from the fuel tank to the combustor. The introduction of heat exchanger(s) (HEX) is therefore necessary for the engines' cycles to benefit from the cryogenic fuel's properties. The fuel heat management system comprises several HEX to transfer heat to the hydrogen fuel to achieve the required temperature before it is injected into the combustion chamber. In practice the several heat exchangers are placed in key locations in the engine core to improve both mechanical and thermal efficiencies of the propulsion system. A reduction of approximately 6% in fuel consumption while increasing the specific thrust have been reported in previous studies [12, 13]. In the design and calculation process of the different HEXs in the engine cycle, in addition to their locations, weights and dimensions are major parameters which must be carefully taken into consideration.

Various heat management concepts using LH_2 as a heat sink will be systematically investigated in ENABLEH2. This requires the development of a modeling environment coupling the cryogenic hydrogen fuel system and turbofan performance. Having separate flow paths for the fuel system and engine core exchanging heat is a challenge that requires appropriate numerical modeling. The model will allow for key parameters in the engine and fuel system design process to be optimized.

Among various alternatives for the fuel heat management architectures in the LH_2 engine's cycle [2, 7, 14], four possibilities arise:

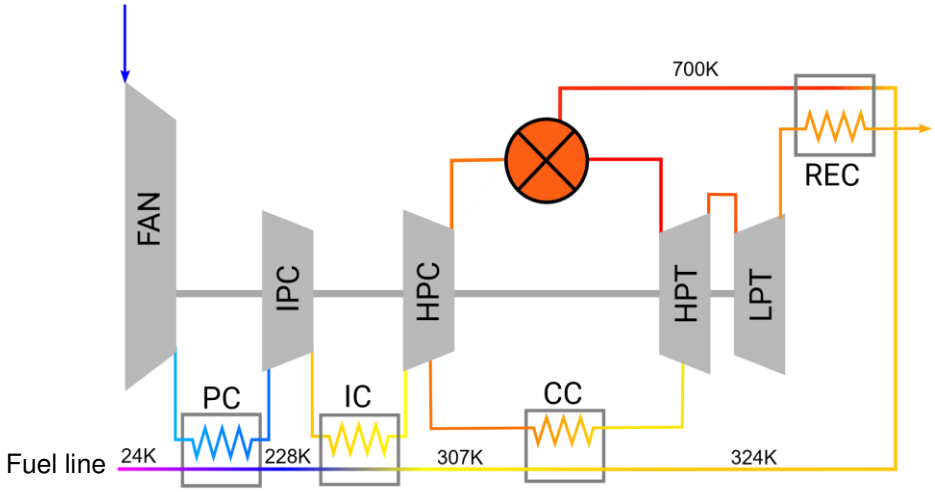

Figure 3: Schematic of fuel heat management system including various HEXs at different engine locations. The diagram also shows the potential fuel temperature variation during take-off.

Pre-cooling (PC) The pre-cooler HEX is located between the fan and Intermediate-Pressure Compressor (IPC). The main roles of pre-cooling are to increase the fuel temperature before entering the combustion chamber and to decrease the IPC and HPC work by cooling the core flow before compression.

Intercooling (IC) The intercooler HEX is placed between the IPC and the High-Pressure Compressor (HPC). Similar to the pre-cooling, the primary roles of intercooling are to raise the fuel temperature before entering the combustion chamber and to reduce the HPC work by cooling the compressed airflow.

Cooled-cooling (CC) The main task of the cooled-cooling HEX is to reduce the temperature of the cooling air extracted from the HPC and used to cool the High-Pressure Turbine (HPT).

Recuperation (REC) The recuperator is the main source of heating the LH_2 fuel before entering the combustor. Among the other HEXs in the LH_2 engine's cycle, it has the greatest potential for increasing the fuel temperature. It is located after the Low-Pressure Turbine (LPT) where it heats up the fuel in the order of 500-600 K.

A schematic illustration of an envisaged heat management architecture integrated into the propulsion system is seen in Figure 4. The figure also shows the potential designs envisaged, ranging from involute spiral tubular to vane-integrated HEX.

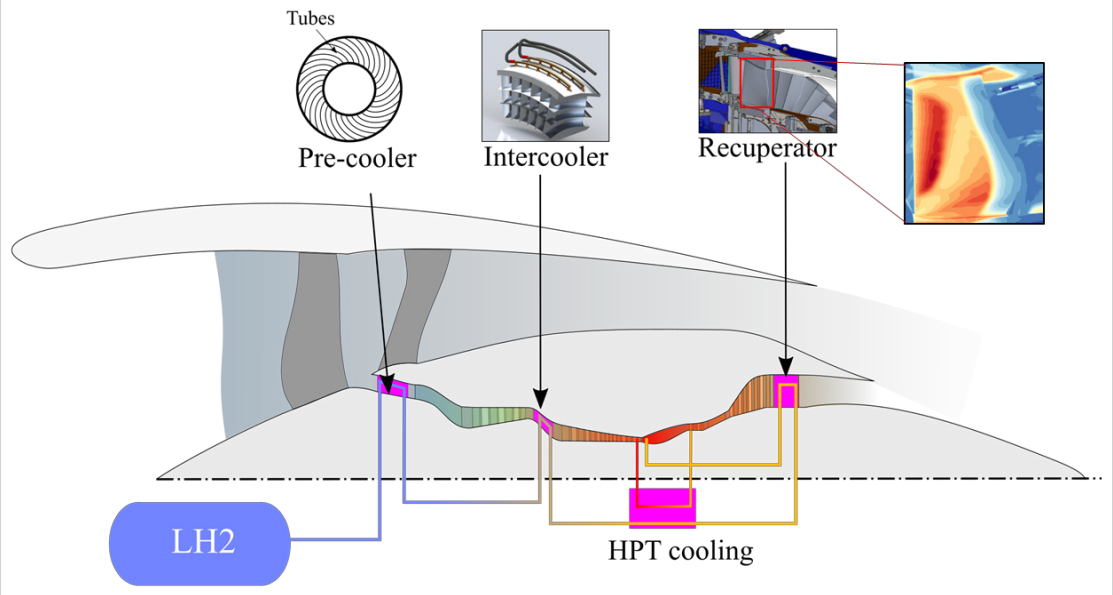

Figure 4: Schematic of fuel heat management system using H_2 as heat sink.

1.2.1 Expander cycle

The role of the expander cycle is to provide the required power for the fuel subsystems by means of a hydrogen expansion turbine. The location of the expansion turbine in the architecture will be the subject of future optimization studies.

Generally, in the expander cycle the pressure of hydrogen fuel is raised to a level higher than that required by the engine. The pressurized hydrogen fuel, passing through the engine is heated up and is expanded while doing work to the turbine. A schematic of the expander cycle can be seen in Figure 5 where the expansion turbine is placed after the precooler.

As seen, it is a closed loop cycle where the fuel temperature increases across the precooler to drive the expansion turbine. The generated torque by the expansion turbine drives the electric generator to provide required power for the pumps in the fuel distribution system and aircraft accessories. The main advantage of the expander cycle is that it does not require any combustion device which in turn increase its simplicity [15]. However, its application is limited to supplying the aircraft and engine subsystems energy requirements. In other words, the power available from the expander cycle is insufficient to provide useful power for the fan or compressors.

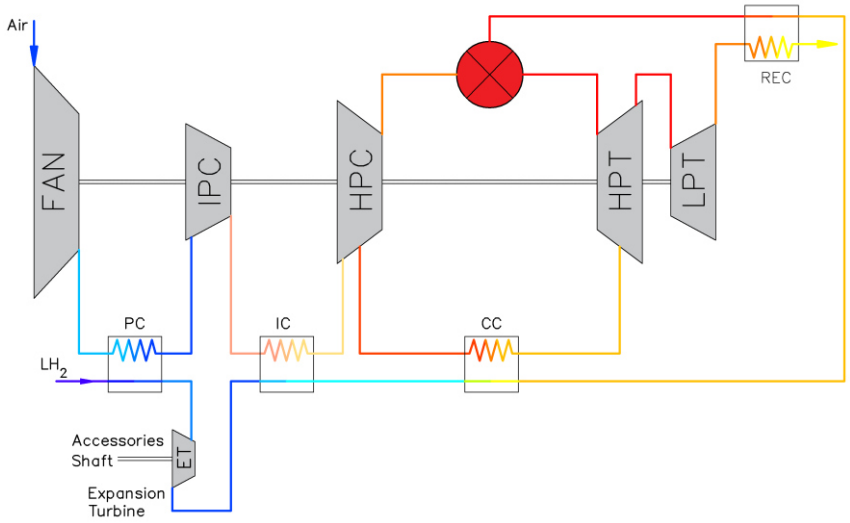

Figure 5: Schematic of fuel heat management system including expander cycle.

1.3 Fuel distribution system

Similar to the conventional Jet A fueled aircraft, the main task of the fuel system for the cryogenic fueled aircraft is to deliver the H_2 with appropriate pressure to the engines for a specified fuel flow. The fuel distribution system, illustrated in Figure 6, consist of different components connected together to supply the hydrogen from the fuel tank to the engine mounted pump (before entering the different HEXs) through the tank-mounted pump(s), inline pump, tank shut-off valve and fuel lines. The proposed fuel distribution system is a multistage pump system where the two major deterministic parameters for the fuel distribution lines are the pipeline diameter and proper insulation system. Technically, these parameters affect the fuel pressure drop (compensated by the tank-mounted and inline pumps) and heat leakage per unit length as well as pipeline weight.

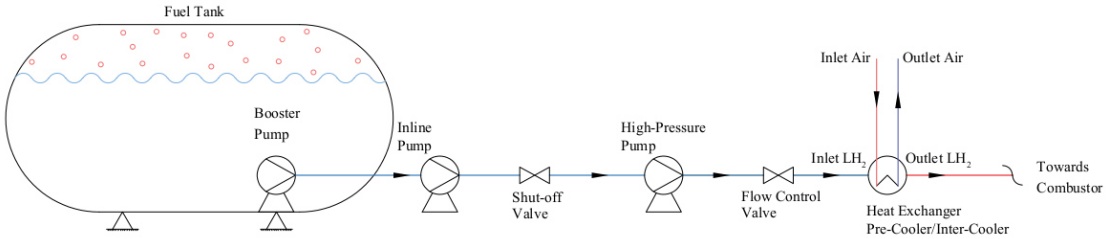

Figure 6: Schematic of cryogenic fuel distribution system

The small pipe size decreases the pipeline weight. However, it increases the pressure drop (especially for maximum fuel flow rate) requiring a larger pump to overcome, which accordingly increases the fuel system's weight. On the other side, apart from minimizing the heat loss, manufacturing/installation cost and maintenance cost, the criterion for the insulation type of the fuel distribution pipeline is not to have ice or dry ice or worse growing on the outside of the insulation or on components adjacent to the pipes and chilled by them. This may require a ventilation system around the pipes, preferably with a dry inert gas from an onboard inert gas system (OBIGS).

A parametric study [2], including a direct operating cost (DOC) estimation, due to the pumps weight and efficiencies, has showed that the fuel supply system must be equipped with two pumps, mounted in the tank and on the engine, respectively. However, in ENABLEH2 we would prefer to design a system that excludes the possibility of having two-phase flow in the fuel line connecting the tank to the engine. Therefore, an additional inline pump is included immediately after the tank to increase the pressure above the critical level. The pressure rise could potentially be achieved by the booster pump (therefore excluding the inline pump). However, a very high pressure rise across the booster pump will affect the

size and efficiency of the pump, the motor power demand as well as additional heat added by the motor inside the tank, therefore it is preferable to include an external high-pressure pump instead. The required fuel pressure delivered to the engine's cycle by the fuel distribution system is therefore divided between the tank-mounted, inline pump, and engine-mounted pumps, see Figure 6. The engine mounted pumps might be included before, after or in-between the different heat-exchangers. The final architecture will be a result of a comprehensive optimization study in task 2.4.

Since the inline pump inlet pressure is equal to the discharge pressure of the booster pump, the inline pump must be rated for the higher suction and discharge pressures. The advantage of higher discharge pressure is that the H_2 would be in supercritical phase condition and does not suffer a phase change. Since the inline pump inlet pressure is equal to the discharge pressure of the booster pump, hence, the inline pump must be rated for the higher suction and discharge pressures. Similar to the boost pump, to avoid the fuel delivery failure due to inline pump damage, spare inline pumps must be foreseen at each fuel line towards the high-pressure pump mounted on each engine. Practically, engines may need to be supplied by more than one fuel tank or switched to different fuel tanks in a failure case. Hence, any one tank should be capable of supplying all the engines so that the total number of booster and inline pumps should be able to cope with these cases. In the parametric study section, the impact of the tank-mounted pump, inline pump and engine-mounted pump on the performance of engine's cycle is studied.

Regarding the type of pump, a comparison of different designs such as inducer, vane, piston and centrifugal pumps [2] revealed that the centrifugal pumps have higher efficiencies, relatively convenient lubrication system and lower weights while they can operate in various design and off-design conditions. However, this is no longer valid while considering the supply systems raises the pressure to supercritical levels. In this case centrifugal pumps could provide lower pressures at lower fuel flows.

In case of using turbo-pumps providing 13 bar plus, the pumps must operate at relatively high speed with relatively high mass flow, which will not always match engine demands. Centrifugal pumps can still be used, but they may need to spill and recirculate excess mass flow, especially if sized to supply two engines, but normally only supplying one. This is less efficient, but it is done today on the engine with kerosene high-pressure fuel pumps. Apart from centrifugal pumps, application of the positive-displacement pump in the fuel distribution systems must be also taken into consideration. The highest reliability, low maintenance and precisely controllable flow are primary benefits of a positive-displacement pump. It cannot generate as high flow rates as a centrifugal pump, but it can operate at high pressures and relatively low flows more efficiently than a centrifugal pump. As an example, existing natural gas fueled gas turbines generally use positive-displacement pumps (piston type) to raise the gas pressure if the pipeline pressure is not high enough. In this initial study and for simplicity, single-stage and constant speed centrifugal pumps are chosen for all pumps in the fuel distribution system.

1.3.1 Boost Pump

The boost pump is located inside the LH_2 fuel tank. According to the regulations prescribed by the Federal Aviation Administration (FAA) in the United States, each engine must be supplied by a separate fuel tank during the take-off (Doc. Fuel Tank Flammability Reduction Means, AC No. 25.981-2A, issue 2008). Contrary to the Jet A fueled aircraft, where the boost pumps rarely operate during the take-off and initial climb, the failure of the boost pump in an LH_2 fueled aircraft leads to fuel vaporization in the fuel delivery line (because of loss of pressure) which in turn may result in an engine failing due to fuel starvation. To prevent loss of thrust on any occasion of boost pump failure, especially at take-off and initial climb, the first scenario is that each tank must be equipped with at least two simultaneous operating pumps and a redundant one. However, the requirement to have the pumps operating simultaneously may be avoided if each engine is fed via a buffer tank containing a reserve of pressurized cold supercritical hydrogen gas. In this case there would be time to start-up the reserve boost pump and/or inline pump before the engine(s) would be starved of fuel. While most aircraft engines today can normally operate on gravity feed alone, without relying on back-up pumps, that is probably not true of center engines on the McDonnell Douglas MD-11 and DC-10, though very few of these aircraft remain in service. In addition, long cylindrical tanks present a further problem in that when a tank is nearly empty of LH_2, then at certain aircraft attitudes, despite internal baffles, the LH_2 may all migrate to one end of the tank. It may be necessary to have boost pumps at both ends of such tanks so that one at least will not run dry. Here some of the redundancy requirements has been consider, however they need careful review.

The fuel pressurized by the boost pump is delivered to the inline high-pressure pump (close to the fuel tank with an appropriately short connecting line) through the fuel lines and valves. The primary duty of the boost pump is to increase the minimum necessary fuel pressure to satisfy the net positive suction pressure (NPSP), i.e., the pressure above the vapor pressure, required by the inline high-pressure pump.

To select the boost pump various parameters such as the pump-driven system (AC/DC motor) and constant/variable speed motor must be considered to fulfill the requirements of fuel delivery through the pipelines and valves to the high-pressure pumps (inline and engine-mounted) with respect to the efficiency and operation range. With a constant speed motor, a single-stage pump can cover a wider operation range relative to a multi-stage pump, but with a lower efficiency. A variable speed motor requires a lower number of stages making it possible to use a high-performance type of pump.

1.3.2 High-Pressure Pump

To pressurize the H_2 fuel before the HEXs or combustion chamber, additional high-pressure pumps are required. The purpose of the high-pressure pump is to provide high-enough fuel pressure for the combustor for various operating conditions while considering the properties of hydrogen characterized by cryogenic temperature, low viscosity and poor lubricity [2].

Previous investigations on high-pressure pump systems revealed that the centrifugal pump is superior to other pump types such as positive displacement piston pump and positive displacement vane pump [2]. Leakage and heavy weight are the main drawbacks of positive displacement piston pumps. Contrary to the positive displacement pumps, centrifugal pumps, either single- or multistage can serve as appropriate types of pump for H_2. In addition, multistage centrifugal pumps have smaller diameter and higher efficiency than single-stage pumps.

In the design of the fuel distribution system, the amount of heat added by the booster and inline pumps and tank immersed electric motor as well as fuel supply line (for the engine mounted pump) must be taken into account. The inlet saturation pressure can be computed as

$$P_{hp\ pump,inlet} = P_{tank} + \Delta P_{bs\ pump} + \Delta P_{inline\ pump} - \Delta P_{feed\ line} \quad (1)$$

where $\Delta P_{bs\ pump}$, $\Delta P_{inline\ pump}$, $\Delta P_{feed\ line}$ denote pressure difference across the booster pump, pressure difference across the inline pump and pressure loss of feed line, respectively. The feed line pressure loss is given by

$$\Delta P_{feed\ line} = f_d \frac{\rho_{LH_2}}{2} \frac{v^2}{D_i} L \quad (2)$$

where f_d, ρ_{LH_2}, L, v and D_i denote the Darcy friction factor, the density of liquid hydrogen, the feed pipeline length, the mean flow velocity in the feed pipeline and the hydraulic diameter of the feed line, respectively.

The inlet enthalpy (h) of the high-pressure pump is given by

$$h_{hp\ pump,\ \ inlet} = h_{tank} + \Delta h_{bs\ pump} + \Delta h_{inline\ pump} + \Delta h_{motor\ bs\ pump} + \Delta h_{feed\ line} \quad (3)$$

where the specific enthalpy change by different pumps is estimated assuming the respective pump efficiency and using REFPROP to compute the reversible process enthalpy states for the prescribed inlet pressure, pressure ratio and inlet entropy as

$$\Delta h = \frac{\Delta h_{ideal}}{\eta} \tag{4}$$

and the enthalpy rise due to the feed line is estimated by

$$\Delta h_{feed\ line} = \frac{q_L L}{\dot{m}} \tag{5}$$

where q_L, $\dot{m}$ denote feed line heat flux per unit length and fuel flow rate, respectively. In this study, it is assumed that $q_L = 20\ \mathrm{W/m}$, $\eta_{bs\ pump} = 0.7$, $\eta_{inline\ pump} = 0.85$ and $\eta_{motor\ pump} = 0.90$.

2 Design Tools

All propulsion modeling carried for this work has been implemented in Chalmers University's in-house gas turbine modeling tool GESTPAN [16]. In addition to basic performance modules commonly available in most performance tools, links exist to external codes for conceptual design and weight estimates as well as for acoustics modeling. The GESTPAN code is a FORTRAN 90 implementation supporting both steady state and transient modeling and is general in the sense that new gas turbine models can be wired up, by freely connecting components to configure a propulsion system. This allows the tool to refine a certain subsystem, connect it in its normal style and model a refined zoomed subsystem with a "normal" gas turbine model for instance for a turbofan engine. This should make the tool ideal for refining existing gas turbine models to include more advanced fuel heat management systems and couple them to the normal air breathing combustion models.

Three additional steps are needed when extending gas turbine performance modeling tools for simulation of cryogenic fuels:

- New combustion products tables are needed to complement conventional kerosene tables normally stored in performance codes;
- The integration of detailed modeling for the heat management system as the cryogenic fuel flows from the tank to the combustor chamber;
- Means to model and manage heat between the fuel system and the propulsion system.

2.1.1 Combustion modeling

The first step consists of performing a relatively well-established procedure typically comprised of generating new temperature dependent tables for key properties using dedicated combustion software such as the chemical equilibrium software CEA [17]. Here, CEA was used to establish tables for hydrogen and methane. Thermodynamic tables for relevant properties such as enthalpy, entropy, specific heat and specific heat ratio were then produced using an interface that automates data generation. Figure 7 shows contour maps illustrating two thermodynamic interpolation tables used in GESTPAN to calculate: a) temperature rise in the combustor with varying inlet temperature and fuel air ratio; b) variation of c_p with fuel air ratio and temperature. The tables are then included as optional fuels along with the frequently used Jet A models. Combustion efficiency and combustion aero performance should be correlated with the data generated in WP3.

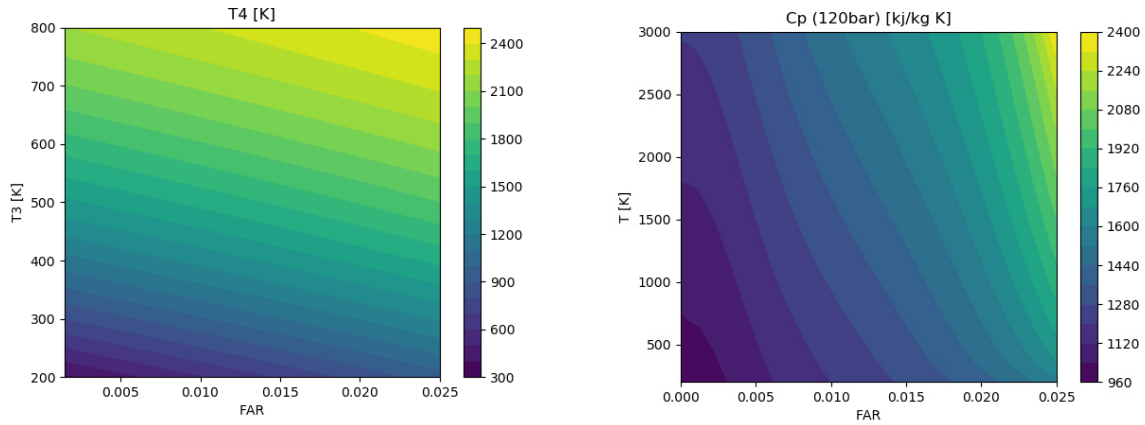

Figure 7: Temperature and FAR (fuel-air ratio) dependent tables for H2. a) Combustion exit temperature; b) Specific heat at constant pressure.

2.1.2 Detailed modeling of real gases

The second step, pure fuel modeling, requires thermodynamic information about the fuel over a very large range, ranging from cryogenic conditions to temperatures considered the maximum for entering the combustor. Here, the extensively used software REFPROP [18] has been applied. Modeling thermodynamics of gases close to the saturation line poses additional difficulties. Most methods used to represent gas data in performance codes are tailored to physics changing rather slowly in the underlying parameters. However, close to the saturation line and especially close to the critical point

changes are often quite rapid and accurate representation using standard spline representation may not be satisfactory. REFPROP has over years developed experience in how to best represent fluids

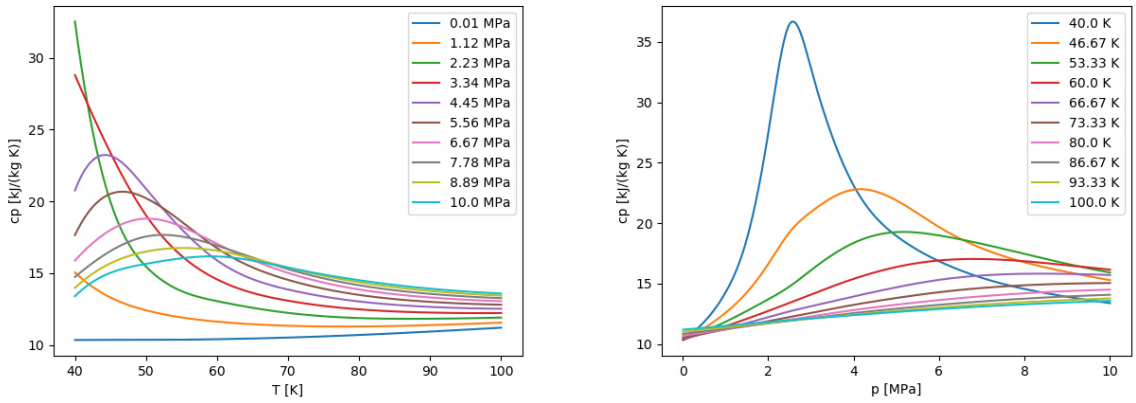

Figure 8: *Variation of specific heat with temperature and pressure.*

accurately around the critical point and it would be reasonable to assume that a direct use of the REFPROP routines linked to the performance code would be the best choice. However, due to speed requirements on REFPROP code, iterative schemes have been included using analytical derivatives of functions. These tend to limit the resolution of the functions and although the software works perfectly in stand-alone mode a directly linked version may fail to work with standard iteration numeric. Hence, the internal iteration schemes of REFPROP have been updated to incorporate methods based on bracketing solutions and using only functional evaluations. These methods are slower, giving a marginal slow-down to the execution, but they are virtually noise free and makes normal gas turbine solutions procedures work well in practice. More specifically, the REFPROP function TPRHO was updated to have more robust and accurate iteration scheme to be used if simulation close to the critical point is being performed. An example of thermodynamic data calculated in GESTPAN for hydrogen is shown in Figure 8. More specifically a variation of heat capacity with temperature and pressure for pure hydrogen is plotted. It is noticeable a large variation of properties occurs close to the critical temperature of 33 K (not present in the plot).

2.1.3 Modeling of coupled heat management systems

The third step, namely heat transfer between the fuel supply and the main engine, poses the greatest modeling challenge. This makes traditional design and off-design simulations of the system substantially more complex to implement. The two flows merging in the main combustor will potentially have exchanged significant amounts of heat prior to fuel injection. Clearly the heat transferred to the hydrogen will be of a magnitude influencing the thermodynamic state of the combustion products. Preheating the fuel from a cryogenic condition of around 25 K possibly all the way up to 800-1000 K requires about up to 14 MJ/kg, i.e., about 10% of the standard state combustion value of the fuel. Conversely, for the air flowing into the engine, even if a typical fuel air ratio for hydrogen combustion will not be more than 1%, this could potentially amount to around a 140 K change in temperature of the working gas.

Conventional software for gas turbine modeling manages the fact that a system of non-linear equations needs to be solved by providing very good starting estimates for the solution. Having a thermodynamic design process indirectly solves this numerical problem. In fact, the design point could be a converged off-design point and hence the method has a built-in solution for defining the first converged point. There is no numerical procedure that promises to achieve this for a general problem. With two separate flows, establishing an “on-design” explicit scheme is not possible. It would be possible to iterate a sequence of converged solutions. This would however be numerically challenging and inefficient since the number of nested iterations in a normal gas turbine code is already at least two, but frequently three or even four. Local iterations to establish thermodynamic gas properties, iterative schemes for Reynolds number corrections etc are commonplace in gas turbine simulation software. Nested around these functions is normally a Newton solver, usually with a secant method for solution, but brute force Newton is still in use in some codes. Many optimizers are iterative, and optimization is a common task for gas turbine simulations. Hence, when for instance cycles are being optimized another iterative level is then required. In addition, many times the thermodynamic design

itself is iterative, matching a thrust or similar. Hence up to four nested iterations already exist in state-of-the-art gas turbine simulation software. It is not practical to add a fifth level. The already large number of nested iterations poses numerical requirements many times not known to users and even to developers, rendering many very efficient optimization methods useless or impractical purely for not fulfilling the numerical requirements of the underlying gas turbine model. To summarize, it is not desirable to add further levels of iterations caused by separate fuel flow systems.

Substantial numerical experimentation was undertaken to consider how to best integrate the fuel heat management system into coupled gas turbine simulations. This experimentation has led to the conclusion that the best way to integrate the fuel heat management system directly is to add additional equations to the thermodynamic design point iterations. For instance, simultaneously varying gas turbine mass flow to match a thrust requirement and iterate in the fuel flow in the heat management system does not increase the number of iteration levels, it merely adds an extra equation of the design iteration system. After realizing that this is how the fuel system should be implemented, many successful studies of coupled fuel heat system and gas turbine system simulations have already been undertaken in ENABLEH2.

2.1.4 Engine template for cryogenic fuels

A wiring diagram for an engine template for the simulation of cryo-fuels is shown in Figure 9 below. The engine includes all the technology and models developed at Chalmers. Switching between different architectures is achieved with component activation flags, supported by the HMS control algorithm. The model is generic and may be used for Jet A, a biofuel, LNG and LH_2.

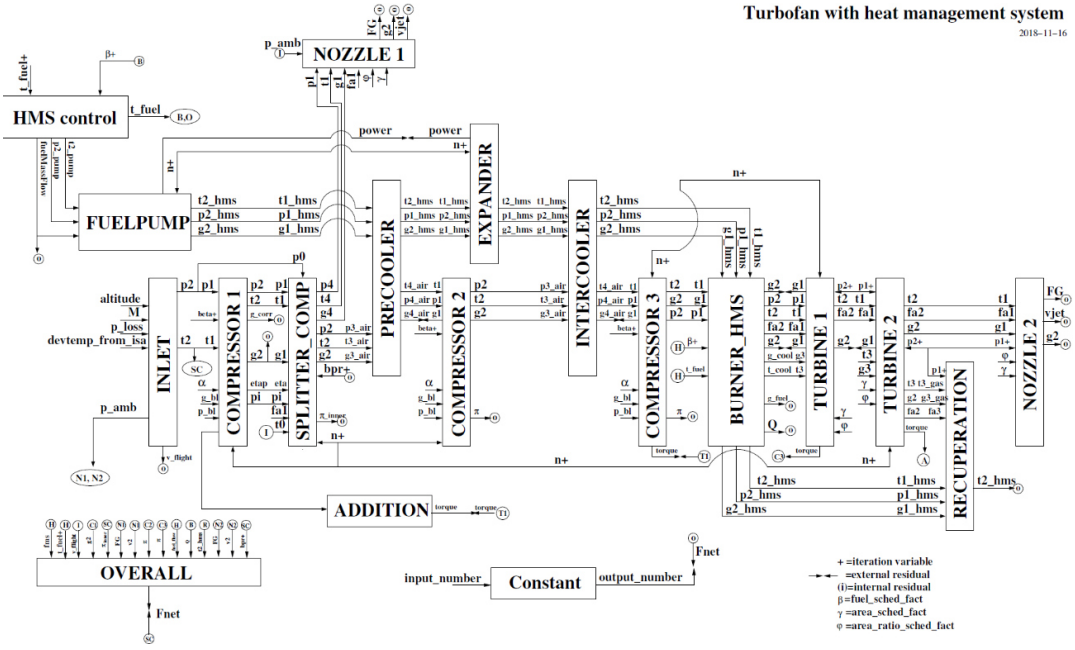

Figure 9: Wiring diagram for coupled turbofan and heat management system

2.1.5 Quantifying installation effects

In the design and calculation process of different HEX architectures in the engine cycles, apart from their overall impacts on the thermodynamic performance, their size, weight and efficiency are major parameters that must be taken into careful consideration. Therefore, instead of Thrust Specific Fuel Consumption (TSFC), another parameter, the so-called installed TSFC ($\overline{TSFC}$) is considered. This takes the drag of nacelle and engine weight into account. In other words, $\overline{TSFC}$ is an actual measure of SFC where the impact of engine installation and relevant losses is counted. It is given by

$$\overline{\mathrm{TSFC}} = \frac{\mathrm{TSFC} * \mathrm{F_n}}{\mathrm{F_n} - \left(\mathrm{D_{Nacelle}} + \mathrm{D_{Engine}}\right)} \tag{6}$$

where F_n, $D_{Nacelle}$, D_{Engine} denote net thrust, nacelle drag and the drag attributable to the engine's weight, respectively. The engine's drag is given by

$$\mathrm{D_{Engine}} = \frac{m_{engine} * g}{(L/D)_{norm}} \tag{7}$$

where m_{engine}, g and $(L/D)_{norm}$ denote engine's mass, gravity acceleration and nominal aircraft lift to drag ratio, respectively.

2.2 Conceptual design of heat exchangers

The advantage of LH_2 in terms of cryogenic storage temperature and high specific heat capacity results in an improved cooling capacity relative to conventional fuels. Adequate heat exchanger technology is therefore required to make use of such benefits.

Heat exchangers are an integral feature of advanced turbofan engine designs. The design of heat exchangers for cryogenic fluid flow is a challenging heat transfer task. Aiming for high-effectiveness accurate design asks for highly precise thermodynamic data and vapor-liquid equilibrium data since the thermophysical properties of cryogenic fluids significantly vary with temperature. On the other hand, the large temperature gradients of the cryogenic and ambient fluids could result in undesirable phenomena such as boiling, condensation, two-phase flow in the heat exchangers [19]. This increases the complexity of thermo-aero-mechanical design and analysis of cryogenic HEX where the utilization of conventional designs is questionable. Among many design parameters for a high-efficiency HEX, particularly in aerospace applications, large surface-to-volume ratio for maximum heat transfer with acceptable pressure losses is a crucial criterion to achieve a design that meets the desired performance.

2.2.1 Generalized approach to model compact HEX technology

Normally, compact heat exchangers (CHEX) are used for large heat transfer surface to volume ratio, especially when one of the mediums is a gas. Depending on the application, either tubular or plate configurations with different fin and tube layouts may be used. In CHEX design, the heat transfer is expressed on the basis of the dimensionless parameters, i.e., Colburn j factor (j), Stanton (St) and Reynolds (Re) numbers. They are defined as

$$\mathrm{j} = \mathrm{St}\,\mathrm{Pr}^{\frac{2}{3}} \tag{8}$$

$$\mathrm{St} = \frac{h}{G c_p} \tag{9}$$

$$Re = \frac{G D_h}{\mu} \tag{10}$$

where G, Pr, h, c_p, D_h and μ denote maximum mass velocity, Prandtl number [-], heat transfer coefficient [W/m^2], specific heat at constant pressure [J/kg-K], hydraulic diameter of flow passage [m] and dynamic

viscosity [kg/m-s], respectively. It is also assumed that c_p is constant or averaged across the heat exchanger. Various types of fin and tube configurations may be used. In most textbooks [20], the performance correlations for CHEX are given as for example in Figure 10.

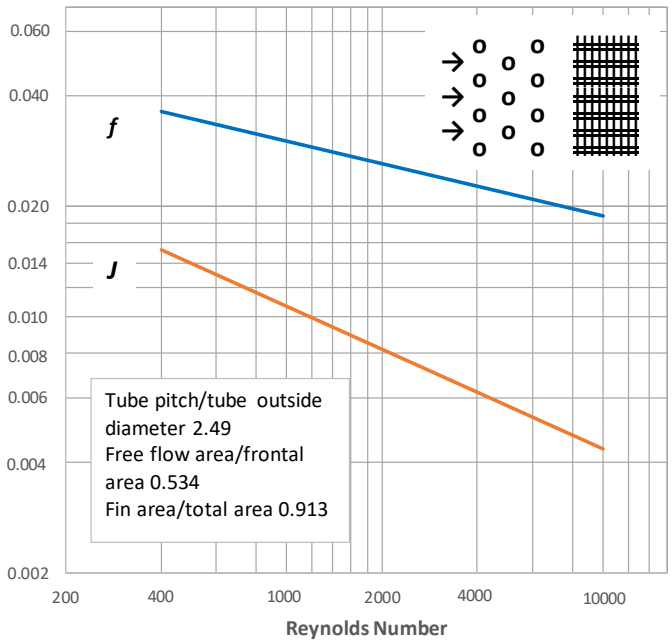

Figure 10: Colburn and friction factors vs. Reynolds number for a circular tube-fin HEX, surface 8.0-3/8T [20, 21]

The Reynolds number is computed based on the maximum mass velocity given by

$$G = \rho V_{max} = \frac{\rho V A_{ft}}{A_{ff}} = \frac{\dot{m}}{A_{ff}} = \frac{\dot{m}}{\sigma A_{ft}} \tag{11}$$

$$\sigma = \frac{A_{ff}}{A_{ft}} \tag{12}$$

where A_{ft} and A_{ff} represent the frontal area and the minimum cross-sectional area perpendicular to flow direction, respectively. The pressure drop across a tubular CHEX design can be expressed as

$$\Delta p = \frac{G^2}{2\rho_i}\left[(1+\sigma^2)\left(\frac{\rho_i}{\rho_o}-1\right) + f\frac{A}{A_{ff}}\frac{\rho_m}{\rho_o}\right] \tag{13}$$

where ρ_i and ρ_o are the density of the inflow and outflow, respectively and $\rho_m = (\rho_o + \rho_i)/2$ is the average density computed on the basis of inflow and outflow densities. In addition, the friction factor f and the ratio of total heat transfer surface to minimum free-flow area A/A_{ff} are determined based on the selected configuration (see Figure 10).

The effectiveness - number of transfer units (ϵ-NTU) method is a robust method to calculate heat transfer performance when only the inlet temperatures are known [21]. In this method, the effectiveness parameter is defined as the ratio between the actual heat transfer rate and the maximum possible heat transfer rate,

$$\epsilon = q/q_{max} \tag{14}$$

The maximum possible heat transfer rate q_{max} depends on a fluid encountering the maximum possible temperature difference $\Delta T_{max} = T_{h,i} - T_{c,i}$, and it is expressed as:

$$q_{max} = C_{min}\left(T_{h,i} - T_{c,i}\right) \tag{15}$$

where C_{min}, $T_{h,i}$ and $T_{c,i}$ represent the minimum heat capacity rate, the gas-side (hot) inflow temperature and the H_2 side (cold) inflow temperature, respectively. The minimum heat capacity rate C_{min} is given by

$$C_{min} = \begin{cases} \dot{m}_c c_{p,c}, & c_{p,c} < c_{p,h} \\ \dot{m}_h c_{p,h}, & c_{p,c} > c_{p,h} \end{cases} \tag{16}$$

where $\dot{m}_c$ and $c_{p,c}$ are H_2 fluid mass flow rate and specific heat at constant pressure while $\dot{m}_h$ and $c_{p,h}$ are gas mass flow rate and specific heat at constant pressure, respectively. For steady flow, the energy equation can be written as

$$q = C_h\left(T_{h,i} - T_{h,o}\right) = C_c\left(T_{c,o} - T_{c,i}\right) \tag{17}$$

where $T_{h,o}$ and $T_{c,o}$ denote hot outflow temperature and cold outflow temperature, respectively. Hence,

$$q = \epsilon C_{min}\left(T_{h,i} - T_{c,i}\right) \tag{18}$$

In addition to effectiveness, the dimensionless parameter expressed in number of transfer units (NTU) can be defined as

$$\mathrm{NTU} = \frac{UA}{C_{min}} \tag{19}$$

where U and A denote overall heat transfer coefficient and heat transfer surface area, respectively. For a single-pass annular heat exchanger where the hydrogen flows inside the tubes, the total cold-side H_2 heat transfer area A_c is calculated based on the number of tubes (N_{tubes}) expressed as

$$A_c = N_{tubes}\pi D_i(R_t - R_h) \tag{20}$$

$$N_{tubes} = \frac{4A_s}{\pi D_i^2} \tag{21}$$

where R_t, R_h, A_s and D_i represent local tip radius, local hub radius, total cross-section area for inner (H_2) flow and tube inside diameter, respectively. The cross-section area for inner flow is computed as

$$A_s = \frac{\dot{m}_c \sqrt{R_{H_2} T_i} \left(1 + \frac{(\gamma - 1)}{2} M_i^2\right)^{\frac{(\gamma+1)}{2(\gamma-1)}}}{P_i \sqrt{\gamma} M_i} \tag{22}$$

where $\dot{m}_c$, R_{H_2}, T_i, γ, P_i and M_i denote inner fluid (H_2) mass flow rate, gas constant, inflow temperature, specific heat ratio of H_2, inflow pressure and the prescribed inflow Mach number, respectively.

For a finless-tube compact heat exchanger, the overall heat transfer coefficient (U_h) of external side (gas/air) is computed as

$$\frac{1}{U_h} = \frac{1}{h_c (A_c/A_h)} + A_h R_w + \frac{1}{h_h} \tag{23}$$

$$\frac{A_c}{A_h} \cong \frac{D_i}{D_o} \tag{24}$$

$$A_h R_w = D_i \frac{\ln\left(\frac{D_0}{D_i}\right)}{2k(A_c/A_h)} \tag{25}$$

where h_c, h_h, A_h, R_w and D_o denote the H_2 side (cold) convection coefficient, gas-side (hot) convection coefficient, total gas-side surface area, tube wall conduction resistance and outside tube diameter, respectively. Moreover, the H_2 and the gas-side convection coefficients are expressed as

$$h_h = j \frac{G c_{p,h}}{Pr_h^{2/3}} \tag{26}$$

$$h_c = \left(\frac{(f/8)\left(Re_{D_i} - 1000\right)Pr}{1 + 12.7(f/8)^{1/2}(Pr^{2/3} - 1)}\right)\frac{k}{D_i} \tag{27}$$

where j_H, G, $c_{p,h}$, Pr_h, Pr, f, k and D_i denote Colburn j factor, maximum mass velocity, gas side (hot) specific heat at constant pressure, gas side (hot) Prandtl number, H_2 Prandtl number, tube friction factor, thermal conductivity of H_2 (cold) and tube internal diameter, respectively. Equation 27 is valid for a large Reynolds number range ($3000 \leq Re_{D_i} \leq 5 \times 10^6$) including the transition region and $0.5 \leq Pr \leq 2000$ where the properties should be taken at $T_m = (T_o + T_i)/2$ which is the average temperature computed on the basis of inflow and outflow temperatures [21]. The tube friction factor f may be also computed from the Moody diagram.

Depending on the HEX flow arrangement, the explicit relation between effectiveness (ϵ) and NTU is introduced in design textbook tables [21]. For example, for a crossflow (single pass) arrangement where one of the fluids is mixed, the effectiveness for C_{max} (mixed) and C_{min} (unmixed) is given by:

$$\epsilon = \left(\frac{1}{C_r}\right)(1 - \exp\{-C_r[1 - \exp(-\mathrm{NTU})]\}) \quad (28)$$

and for C_{max} (unmixed) and C_{min} (mixed) is given by:

$$\epsilon = (1 - \exp(-C_r^{-1}\{1 - \exp[-C_r(\mathrm{NTU})]\})) \quad (29)$$

where $C_r = {C_{min}}/{C_{max}}$.

During design the ϵ-NTU method is used to compute the heat transfer surface area, volume and weight for a desired effectiveness. For this purpose, in addition to the selection of a particular geometry, air/H_2 inflow rates and temperatures, the effectiveness (ϵ) of the CHEX are prescribed.
In the proposed design approach, the effectiveness is prescribed to compute the minimum tube diameter for H_2 flow, through an iterative process that in turn yields the total number of tubes. The constraint for the minimum tube diameter is the H2 flow velocity inside the tubes. Geometrical parameters of a chosen CHEX configuration such as σ (free-flow area/frontal area, see Figure 10), α (heat transfer area/total volume) and D_h (flow passage hydraulic diameter), are scaled within the iteration for the varying tube diameter. In addition, based on the thermodynamic properties of air and H_2, as well as the scaled physical properties of the selected CHEX, the convective heat transfer coefficients for both external (air) and internal (H_2) flows are determined (see Equations 26 and 27). The number of tubes, the frontal area and the extracted parameter α based on the CHEX configuration yield the tube length. Depending on the specified tube material, heat exchanger mass is computed. To meet the temperature limits of ASME B31.12 (Standard on Hydrogen Piping and Pipelines), austenitic (300 series) stainless steels are recommended for piping in gaseous and liquid hydrogen services. Among different grades (such as type 304L and type 321), stainless steel type 316/316L is the most stable grade with relatively high-resistance to hydrogen embrittlement when exposed to high pressure hydrogen.

In the above calculation procedure, it is assumed that the heat capacity (c_p) is constant and does not vary significantly with temperature. In connection to Figure 1, the inclusion of high-pressure pumps before the HEX reduces the relative jump in specific heat of hydrogen in the vicinity of the critical point, making the constant specific heat assumption across the HEX more plausible. Practically, a high pressure of H_2 at the inlet of any HEX is achieved by the inline and HP pumps.

Instead of a conventional tubular heat exchanger with a staggered layout, two new configurations are proposed for the pre-cooler and intercooler. It must be noted that all calculations have been made based on the CHEX with the staggered tube configuration [20]. To study the feasibility of using guide vanes inside the IGVs or OGVs, it is assumed that the two proposed configurations have the same performance as the staggered layout used for HEX sizing. This simplification e.g., for the first layout, neglects the thermal resistance of the conduction path from the tube walls to the outside surface, and also the effect of staggered tubes on turbulence intensity and enhanced heat transfer performance.

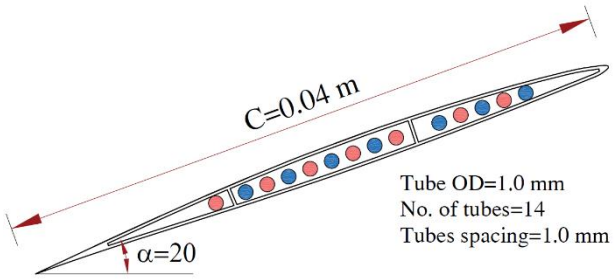

Figure 11: Schematic of the first configuration layout of pre-cooler hex tubes inside IGV stators with chord length c=0.04 [m], blue: inflow, red: outflow.

Figure 11 displays a schematic of CHEX tubes arrangement where a two-pass cross-flow U-shape tubes may be located inside the Inlet Guide Vanes (IGVs) of the IPC for the pre-cooler or inside the Outlet Guide Vanes (OGVs) of the IPC for the intercooler of the reference engine (see section 3). The height and pitch angle of the stators are equal to 0.11 m, and 20 degrees, respectively, therefore, for an aspect ratio of 3 a chord of 0.04 m is obtained. Practically, an array of 1.0 mm tubes ID with 0.05 mm thickness is assumed to be fitted inside the guide vanes with 1.0 mm spacing between the tubes yielding seven U-tubes per guide vane. In an ideal heat-transfer case, a couple of hundred guide vanes must be installed to provide the required surface areas for the pre-cooler and intercooler separately, which would introduce additional wetted surface area for the current turbofan engine. The flow blockage is also a lot higher than for normal compressor designs and would have to be accounted for.

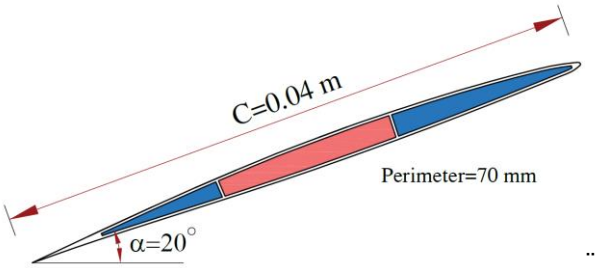

Figure 12: Schematic of alternative layout of pre-cooler using hollow sparred guide vanes. Blue: inflow, red: outflow.

Alternatively, a configuration as shown in Figure 12 could be used, where instead of having tubes inside the IGVs or OGVs, the internal surfaces of the hollow guide vanes provide the heat transfer surface area. The main advantage of this layout is use of the whole surface area around the leading edge of each guide vane where the maximum heat transfer takes place. For the turbofan engine in this study, the inside perimeter of each guide vane is about 0.07 m resulting in 0.007 m^2 heat transfer surface area per guide vane. Hence, for the second proposed configuration, fewer guide vanes are required for both the pre-cooler and the intercooler, relative to the first configuration. Nevertheless, it is still infeasible with respect to providing the sufficient area for a typical IGV blade row count.

3 Parametric study

The present chapter reports on a parametric study used to test the implementation of the new tools and methods for predicting the performance of liquid hydrogen-fueled gas turbine engines. The chapter starts by presenting a baseline engine, optimized to operate on H_2 without including any HEX technology. Afterwards, a parametric sensitivity analysis on two particular concepts for heat recovery, namely pre-cooling and intercooling, is performed to identify the important design aspects of compact heat exchanger technology for cryofueled gas turbine engines.

3.1 Reference optimized cycle

In the analysis of the engine's cycle characteristics, the LH_2 fueled engine (without any HEX) is assessed first to find the optimal FPR and BPR for the minimum $\overline{TSFC}$ (installed TSFC) in cruise conditions. The assumption of no HEX is only made for comparison knowing that its negative impact on the cycle's performance because of reduction of fuel's effective heating value. For this purpose, simulations are performed to predict the design and off-design performance of a commercial year 2020 turbofan engine for short-medium range aircraft. A prescribed mission range is assumed, while the Mach number and typical cruise altitude are set to be 0.78 and 10,058.4 m (33,000 ft), respectively. A summary of the performance data assumptions is presented in Table 4.

Table 4: Year 2020 engine performance data assumptions at SLS ISA take-off condition.

Item	Efficiency [%]
Fan efficiency (isentropic, cruise)	91.5
Booster efficiency (polytropic)	91.0
Cooling-air/core-inlet mass flow	18.0
HPC efficiency (polytropic)	90.0
HPT (isentropic)	90.0
LPT efficiency (isentropic)	92.5

The numerical simulations are performed over various FPR and BPR values to optimize the low-pressure system for minimum $\overline{TSFC}$ while the equivalent cruise net thrust (FN) and ISA-day turbine inlet temperature (TIT) are set to 21.35 kN and 1710 K, respectively. According to Figure 13 for the optimized LH_2 fueled reference engine, the FPR and bypass ratio (BPR) are taken as 1.46 and 14.60, respectively. It must be noted that the selected FPR and BPR are based on the fan size constraint compatible with a commercial year 2020 turbofan engine.

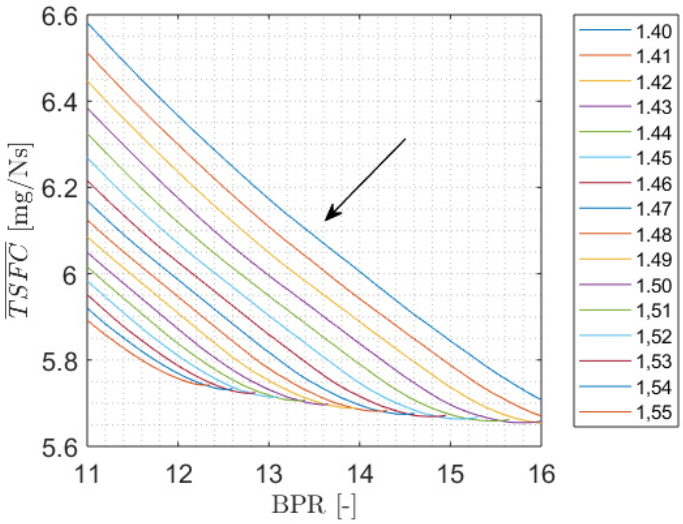

Figure 13: Installed TSFC ($(TSFC)\overline{\ }$) vs. BPR at different FPRs to find the optimum performance point for the LH2 reference engine's cycle. The arrow is related to the legend indicating the direction of increase in FPR from 1.40 to 1.55.

Table 5 displays the cycle performance data for the reference LH_2 SMR at its optimal values of FPR.

Table 5: Comparison of engine parameters with identical Net Thrust (FN) at different ISA-day flight conditions for the reference engine model burning hydrogen.

Item	Flight Condition			
	Take-off	Top of climb	Initial cruise	End cruise
Mach [-]	0.00	0.78	0.78	0.78
Altitude [m]	0.0	10058.4	10058.4	10668.0
FPR [-]	1.46	1.52	1.43	1.42
BPR [-]	14.60	14.54	16.06	16.30
OPR [-]	42.19	48.81	40.76	39.62
Overall efficiency [-]	-	0.38	0.38	0.38
Air flow rate [kg/s]	568.98	266.54	252.14	229.20
Fuel flow rate [kg/s]	0.375	0.156	0.124	0.107
Net thrust [kN]	146.78	30.69	24.46	21.35
TSFC [mg/N.s]	2.55	5.08	5.07	5.04
TIT [K]	1710	1567	1485	1450
Fuel pressure in storage tank [bar]	1.6			
Pumps pressure ratio	30			
Fuel temperature in storage tank [K]	22.02			
Fuel temperature [K]	24.53	24.75	24.85	24.91
Fan diameter [m]	1.98			
Total engine weight [kg]	3262.67			

For comparison Table 6 presents a summary of engine parameters for the (SMR) engine technology burning Jet A.

Table 6: Comparison of engine parameters with identical Net Thrust (FN) at different ISA-day flight conditions for the reference engine model burning Jet A.

Item	Flight Condition			
	Take-off	Top of climb	Initial cruise	End cruise
Mach [-]	0.00	0.78	0.78	0.78
Altitude [m]	0.0	10058.4	10058.4	10668.0
FPR [-]	1.46	1.52	1.44	1.42
BPR [-]	11.25	11.21	12.36	12.55
OPR [-]	40.54	45.12	37.69	36.60
Overall efficiency [-]	-	0.38	0.38	0.38
Air flow rate [kg/s]	530.40	240.25	227.05	206.31
Fuel flow rate [kg/s]	1.09	0.43	0.34	0.29
Net thrust [kN]	146.78	30.69	24.46	21.35
TSFC [mg/N.s]	7.43	14.13	14.00	13.91
TIT [K]	1710	1547	1456	1420
Fan diameter [m]	1.98			
Total engine weight [kg]	3237.59			

3.2 Results

The aerothermal impacts of effectiveness and internal flow velocity on HEX sizing and performance are quantified in the present parametric study. It is assumed that the HEX effectiveness at the design point varies between 0.3 and 0.8 while the velocity at the inlet of HEX tubes at the design point is bounded between 1.0−20.0 m/s. Moreover, in this study, a staggered tube bank configuration, as seen in Figure 14 [20], is used as a generic model while the physical properties are scaled on the basis of the tube diameter. The main focus is directed towards the net benefit by pre-cooling and intercooling because of the potential for re-optimizing the cycle for this type of heat sink is greater. However, due to

the lower temperature of the compressor air, maximum benefits can only be achieved by combining an optimized compression system with a higher temperature source such as cooled cooling or core exhaust heat.

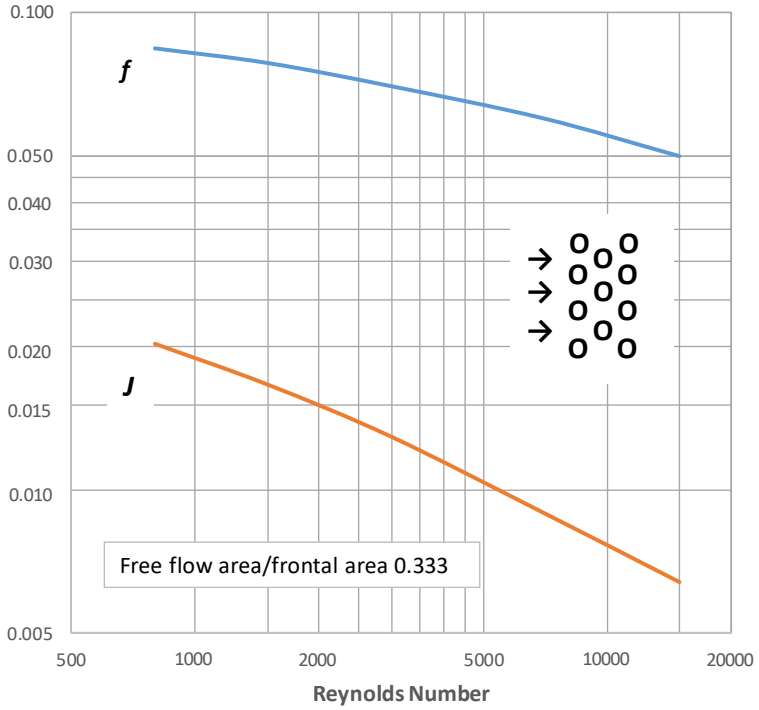

Figure 14: A generic staggered tube bank configuration (S 1.50-1.25(a)) for steady state flow

In addition to the impact of HEX locations on the overall efficiency of the cycle, calculation of size, weight, and efficiency of these HEXs is one of the most important tasks while designing the hydrogen-fueled propulsion system. To assess the individual impact of each HEX in the performance and efficiency of the engine's cycle, numerical simulations are performed for the adapted LH_2 engine's cycle, while in all cases the net thrust (F_N), design FPR, design OPR and design TIT are kept constant. Parametric variations are therefore carried out with the same efficiency and technical assumptions for the reference engine and the engines with pre-cooler and intercooler. Actually, the different architectures are configured using the same model, since the setup only differs on the parameters used for the design effectiveness and the velocity at the inlet of HEX tubes of both the pre-cooler and intercooler components.

The LH_2 is assumed to be stored at 1.6 bar and 22 K. As seen from Figure 6 the pressure and temperature of the LH_2 is increased during transfer from the storage tank to either the pre-cooler or intercooler HEXs or possibly in sequence. The pressure rise in the boost pump (tank-mounted) and inline/high-pressure pump is equal to 2.5 and 24.5, respectively. Table 7 presents a summary of pre-cooler and intercooler operating conditions under the current pressure rise at the design operating condition.

Table 7: pre-cooler and intercooler HEXs operating conditions

HEX type	Pressure rise	$\Pi_{booster\ pump}$	2.5
		$\Pi_{high\text{-}pressure\ pump}$	24.5
Pre-cooler	LH_2	Inlet pressure [bar]	97.80
		Inlet temperature [K]	24.6
		Flow rate [kg/s]	0.38
	Air	Inlet pressure [bar]	1.31
		Inlet temperature [K]	313
		Flow rate [kg/s]	41.1
Intercooler	LH_2	Inlet pressure [bar]	97.80
		Inlet temperature [K]	24.6

		Flow rate [kg/s]	0.38
	Air	Inlet pressure [bar]	2.22
		Inlet temperature [K]	369
		Flow rate [kg/s]	41.2

Figure 15 shows the geometrical properties of the pre-cooler (at the end-cruise operating condition) in terms of different effectiveness and LH2 flow velocity at the inlet of HEX tubes at the design point. In order to achieve a higher HEX effectiveness, more surface area (expressed by NTU) is required, which is consistent with Equation 19. The pre-cooler is located in the annulus area defined by R_t and R_h (IPC hub and tip radius, respectively). Hence, the frontal area of the chosen CHEX with the staggered tube configuration is expressed as

$$A_{fr} = \pi(R_t^2 - R_h^2) \tag{30}$$

In this study, $R_h = 0.23\ m$ and $R_t = 0.53\ m$. To achieve the required effectiveness, a relatively very large number of tubes is needed. Also, the staggered tubular design results in small tube diameters ranging from 0.1 to 2.0 mm, indicating an impractical HEX configuration given the high air-side pressure loss and risk of foreign object impact damage to the small tubes. It must be noted that in addition to a reduction of specific heat capacity (c_p) at higher pressure, the main reason for the very small tube diameters appearing at high pressures is because of the HEX design procedure (See subsection 2.2.1) where the code iterates on tube diameter for a given effectiveness.

The impact of inline and high-pressure engine mounted pumps on the HEX sizing is shown in Figure 15.

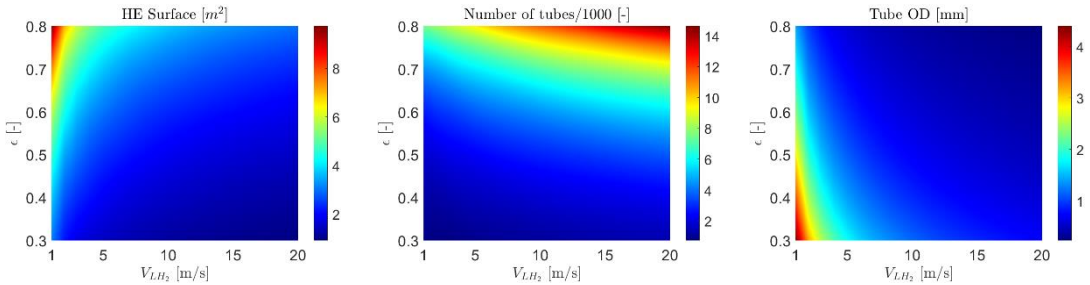

Figure 15: Required HEX surface area, tubes outside diameter and number of tubes at the end cruise condition for varying effectiveness and flow velocity at the inlet of the HEX tubes at the design point of pre-cooler.

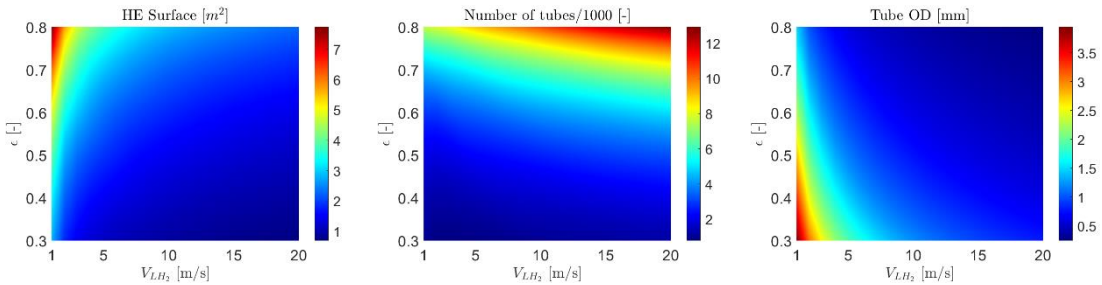

Figure 16: Required HEX surface area, tubes outside diameter and number of tubes at the end cruise condition for varying effectiveness and flow velocity at the inlet of the HEX tubes at the design point of intercooler.

The available annulus area to install the intercooler between the IPC and HPC was estimated based on the hub and tip radii of the HPC. For the reference engine used in this study, the entry hub radius (R_h) and tip radius (R_t) at the exit of the IPC are equal to 0.18 m and 0.43 m, respectively. Therefore, the frontal area (A_{fr}) for the staggered tubular CHEX can be computed as was done for pre-cooler. Because of the smaller hub and tip radii of the HPC, a smaller installation frontal area for the intercooler

is estimated. On the other hand, Figure 15 and Figure 16 reveal that both the pre-cooler and intercooler require almost the same surface area.

The present analysis shows that pressure plays a crucial role in the performance of the H_2 heat exchangers. This indicates that the location of the different pumps in the fuel distribution and heat management system is a critical aspect in design. The down-selection of an optimal system is not in the scope of the present report, and it will be analysed in task 2.4. Therefore, for the remaining analysis only the results obtained with Case 1 will be presented and discussed.

3.2.1 Pre-cooler HEX performance

The impact of higher effectiveness, obtained by a larger surface area, on air and H_2 temperature differences across the pre-cooler is clearly seen in Figure 17, where $\Delta T_{air} = T_{air,out} - T_{air,in}$ and $\Delta T_{LH_2} = T_{LH_2,out} - T_{LH_2,in}$. A higher effectiveness provides more heating for H2 and more cooling for the air. However, it undesirably increases the pressure drop for both the air and the H_2 sides, and especially for the air-side because of a relatively large number of tubes (see Figure 18). A considerable air pressure drop of about 7-22% occurs for an effectiveness greater than 0.7 as seen from Figure 18. In addition, Figure 17 shows the temperature differences across the pre-cooler, for both air and H_2, are proportional to the HEX effectiveness, but independent of the flow velocity at the inlet of the HEX tubes. Figure 15 shows that by lowering the internal flow velocity of the HEX, the required HEX surface area increases, which leads to increasing air-side pressure drop ratios as shown in Figure 18.

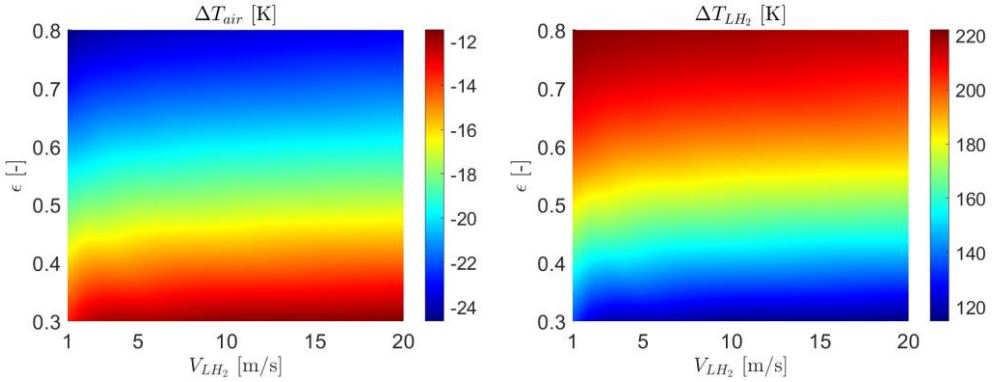

Figure 17: Pre-cooler HEX performance (at the end cruise condition): temperature difference for varying HEX effectiveness and flow velocity at the inlet of the HEX tubes at the design point, left: Air, right: LH_2

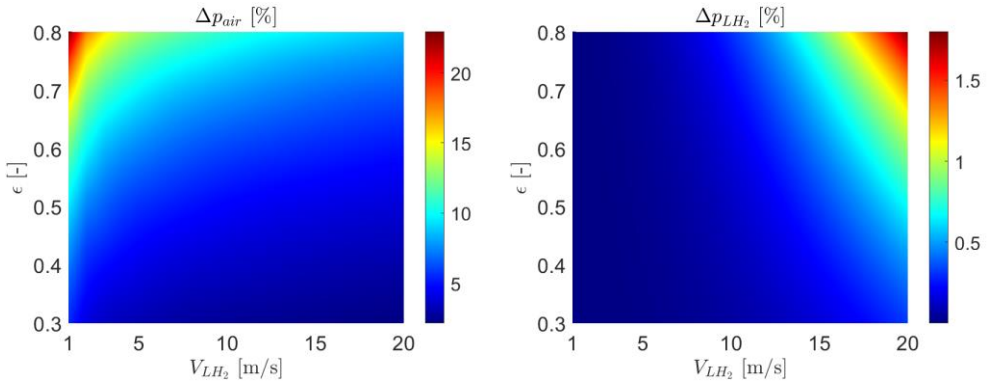

Figure 18: Pre-cooler HEX performance (at the end cruise condition): pressure drop percentage for varying HEX effectiveness and flow velocity at the inlet of the HEX tubes at the design point, left: Air, right: LH2

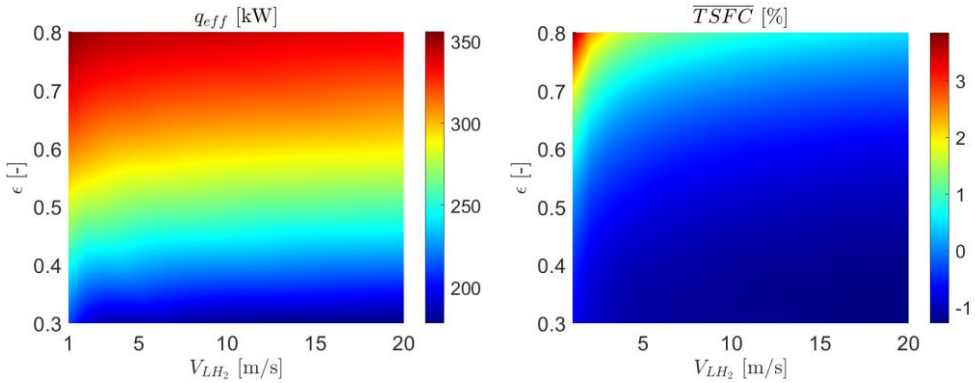

Figure 19: Pre-cooler HEX performance (at the end cruise condition): effective heat transfer and relative $(TSFC)^-$ for varying effectiveness and flow velocity at the inlet of the HEX tubes at the design point.

Figure 19 gives the variation of installed TSFC relative to the optimized LH_2 engine cycle, for varying HEX effectiveness and flow velocity inside the HEX tubes at design condition. As illustrated, the pre-cooler hardly improves the overall performance of the engine's cycle in design. Especially for higher HEX effectiveness, it has a negative impact on the overall performance of the engine due to excessive pressure losses that are not outweighed by the increased fuel temperature and reduced work in the compressors. It is noted that the engine was not re-optimized for operation with a pre-cooler. Still, at high effectiveness the excessive pressure losses are also likely to deny any benefits arising from a cycle optimization, recalling that for each 1% loss in air pressure, there would be approximately 0.3% loss in SFC.

3.2.2 Intercooler HEX performance

Figure 20 show the performance of the intercooler (at the end-cruise operating condition) for various ranges of effectiveness and LH_2 velocity at the inlet of the HEX tubes at the design point associated with the take-off operating condition with the inlet air and H_2 temperatures equal to 369 K and 24.6 K, respectively. Assuming that no expander turbine is placed before the intercooler, the H_2 inlet temperature is the same as the one for the pre-cooler. Similar to the pre-cooler, a higher effectiveness yielding a larger HEX surface area makes larger temperature changes across the intercooler on both air and H_2 sides as demonstrated in Figure 20. However, it increases the pressure drop for both air and H_2 flows (see Figure 21). For the low flow velocity at inlet of the HEX tubes, higher effectiveness of the intercooler causes the air-pressure-drop ratio higher than in the pre-cooler, but the pressure-drop-ratio for the internal flow is almost identical.

Like in the pre-cooler, the temperature difference is independent of the flow velocity at the inlet of the HEX tubes with respect to the HEX effectiveness across the intercooler, as seen in Figure 20. However, the temperature difference across the intercooler for both internal and external flows is almost 20-30% higher than that of the pre-cooler.

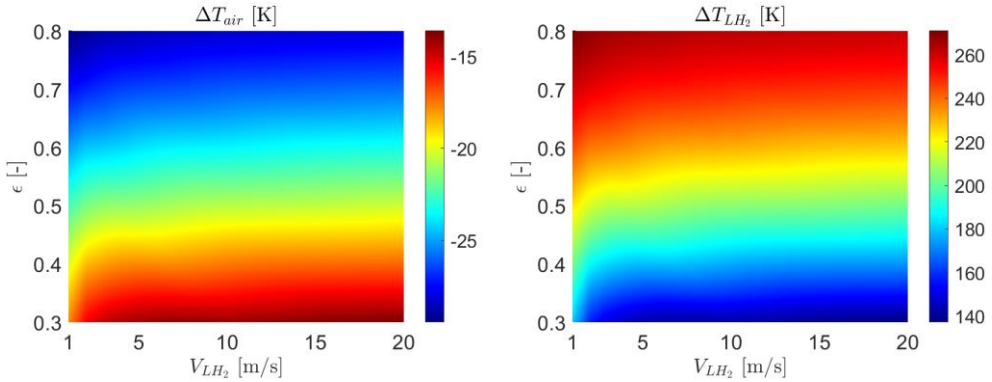

Figure 20: Intercooler HEX performance (at the end cruise condition): temperature difference for varying HEX effectiveness and flow velocity at the inlet of the HEX tubes at the design point, left: Air, right: LH_2

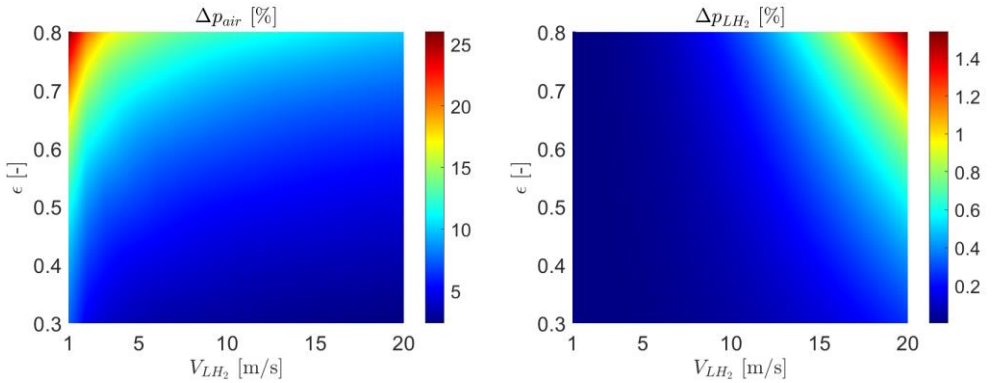

Figure 21: Intercooler HEX performance (at the end cruise condition): pressure drop percentage for varying HEX effectiveness and flow velocity at the inlet of the HEX tubes at the design point, left: Air, right: LH_2

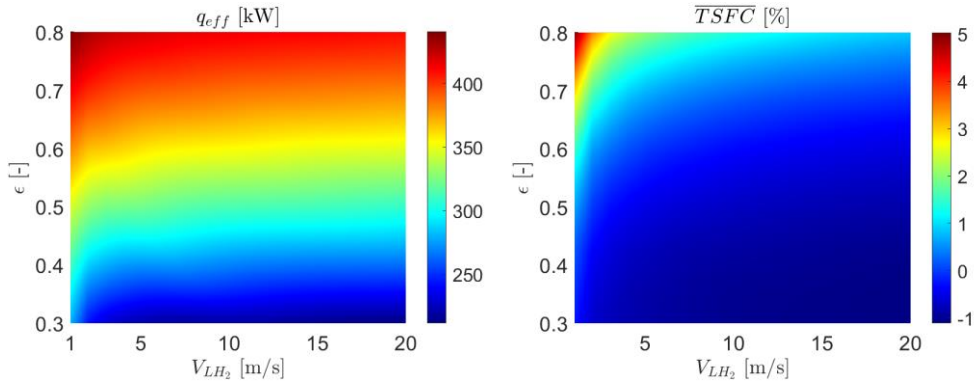

Figure 22: Intercooler HEX performance (at the end cruise condition): effective heat transfer and relative $\overline{TSFC}$ for varying effectiveness and flow velocity at the inlet of the HEX tubes at the design point.

Figure 22 presents the variation of installed TSFC relative to the optimized LH_2 engine cycle, for varying HEX effectiveness and flow velocity at the inlet of the HEX tubes. Like the pre-cooler, intercooler does not reveal substantially positive impact on the engine performance for a broad range of HEX effectiveness levels. In this study, the improvement in $\Delta\overline{\mathrm{TSFC}}$ is limited up to 1.0%, however by optimizing the engine's cycle with a prescribed intercooler HEX, a greater reduction in $\overline{\mathrm{TSFC}}$ is expected.

3.3 Conclusion

For the first configuration layout of HEX tubes inside IGV/OGV stators, a couple of hundred guide vanes must be installed to provide the required surface area for the pre-cooler and intercooler separately. However, this is likely impractical because of the blockage of the air flow and a requirement on the compressor design. Also, the extra wetted surface will lead to a concept that does not perform close to the maximum possible for such an installation. A better alternative, albeit more complex would be to use several stator rows. For the second proposed configuration, with sparred hollow vanes, fewer guide vanes are required for both the pre-cooler and the intercooler. Nevertheless, a multistage configuration would be needed also for this design.

Tube banks such as shown in Figure 14 are compact but do not offer the lowest air-side pressure losses. Profiled tubes and different arrangements can approximately halve the loss but are likely to be heavier.

The pre-cooler hardly improves the overall performance of the engine's cycle in design. Especially for a higher HEX effectiveness, it has a negative impact on the overall performance of the engines due to excessive pressure losses that are not outweighed by the increased fuel temperature. Apart from higher pressure losses by a pre-cooler (because of a higher air-side inlet Mach number), the problem of icing-up of the vanes if the incoming air is at all humid may lead to the conclusion that pre-cooling is not worth further study.

Like the pre-cooler, intercooler does not reveal substantially positive impact on the engine performance for a broad range of HEX effectiveness levels. In this study, the improvement in $\Delta\overline{\mathrm{TSFC}}$ is limited up to 1.0%, however by optimizing the engine's cycle with a prescribed intercooler HEX, a greater reduction in $\overline{\mathrm{TSFC}}$ is expected.

There is a potential to preheat hydrogen more economically elsewhere in the cycle (e.g., combination of intercooling and then preheating the hydrogen in the turbine exhaust) instead of in the pre-cooler/intercooler. In the next step, the benefit of heating the hydrogen before going into the combustor (recuperator HEX) will be studied. The impact of an expander cycle on the engine's performance will be investigated too.

4 Bibliography

[1] A. Westenberger, "Hydrogen Fueled Aircraft," in *AIAA International Air and Space Symposium and Exposition: The Next 100 Years*, Dayton, Ohio, 2003.

[2] G. D. Brewer, Hydrogen Aircraft Technology, CRC Press, 1991, p. 448.

[3] B. Khandelwal, A. Karakurt, P. Sekaran, V. Sethi and R. Singh, "Hydrogen powered aircraft: The future of air transport," *Progress in Aerospace Sciences,* vol. 60, pp. 45-59, 2013.

[4] D. Verstraete, "The Potential of Liquid Hydrogen for long range aircraft propulsion," Cranfield University, Cranfield, UK, 2009.

[5] J. Green, "Greener by Design — the technology challenge," *The Aeronautical Journal,* vol. 106, no. 1056, pp. 57-113, 2002.

[6] H. G. Klug and R. Faass, "CRYOPLANE: hydrogen, fueled aircraft—status and challenges," *Air & Space Europe,* vol. 3, no. 3-4, pp. 252-254, May-August 2001.

[7] F. Svensson and R. Singh, "Effects of Using Hydrogen on Aero Gas Turbine Pollutant Emissions, Performance and Design," in *ASME Turbo Expo 2004: Power for Land, Sea, and Air*, 2004.

[8] H. Rogers, D. Lee, D. Raper, P. Foster, C. Wilson and P. Newton, "The impacts of aviation on the atmosphere," *The Aeronautical Journal,* vol. 106, no. 1064, pp. 521-546, 2002.

[9] F. Haglind, A. Hasselrot and R. Singh, "Potential of reducing the environmental impact of aviation by using hydrogen Part I: Background, prospects and challenges," *The Aeronautical Journal,* vol. 10, no. 1110, pp. 533-540, 2006.

[10] M. Klell, "Storage of Hydrogen in the Pure Form," in *Handbook of Hydrogen Storage: New Materials for Future Energy Storage*, D. M. Hirscher, Ed., 2010, pp. 1-37.

[11] W. L. S. J. L. ,. B. J. G. Staats, "Analysis of a Supercritical Hydrogen Liquefaction Cycle," in *16th International Cryocooler Conference*, Atlanta, Georgia, 2008.

[12] S. Boggia and A. Jackson, "Some Unconventional Aero Gas Turbines Using Hydrogen Fuel," in *Proceedings of the ASME Turbo Expo 2002: Power for Land, Sea, and Air*, 2002.

[13] S. Boggia and K. Rüd, "Intercooled Recuperated Gas Turbine Engine Concept," in *41st AIAA/ASME/SAE/ASEE Joint Propulsion Conference & Exhibit*, Tucson, Arizona, 2005.

[14] I. van Dijk, G. Rao and J. van Buijtenen, "Stator cooling & hydrogen based cycle improvements," in *XIX International Symposium on Air Breathing Engines 2009 (ISABE 2009)*, Montreal, Canada, 2009.

[15] Y. Mack, R. Haftka, L. Griffin, L. Snellgrove, D. Dorney, F. Huber and W. Shyy, "Radial Turbine Preliminary Aerodynamic Design Optimization for Expander Cycle Liquid Rocket Engine," in *42nd AIAA/ASME/SAE/ASEE Joint Propulsion Conference & Exhibit*, Sacramento, California, 2006.

[16] T. Grönstedt, Development of methods for analysis and optimization of complex jet engine systems, Gothenburg, Sweden: Chalmers University of Technology, 2000.

[17] G. Sanford and B. McBride, "Computer program for calculation of complex chemical equilibrium compositions and applications. Part 1: Analysis," NASA, 1994.

[18] E. W. Lemmon, M. O. McLinden and M. L. Huber, "NIST reference fluid thermodynamic and transport properties–REFPROP," National Institute of Standards and Technology (NIST), Boulder, Colorado, 2002.

[19] K. D. Timmerhaus and R. J. Schoenhals, "Design and selection of cryogenic heat exchangers," in *Advances in Cryogenic Engineering*, vol. 13, New York, Springer Science+Business Media New York, 1995, pp. 445-462.

[20] W. Kays and A. London, Compact Heat Exchangers, 3 ed., New York: McGraw-Hill, 1984.

[21] F. Incropera, D. Dewitt, T. Bergman and A. Lavine, Fundamentals of Heat and Mass Transfer, 6 ed., John Wiley & Sons, Inc., 2007.

ENABLEH2

Public Report

Heat management system conceptual design tools report

Authors

Hamidreza Abedi, Tomas Grönstedt, Carlos Xisto, Chalmers University

Andrew Rolt, Cranfield University

This project has received funding from the European Union's Horizon 2020 research and innovation programme under **grant agreement no 769241**